The Heme Pocket Geometry of *Lucina pectinata* Hemoglobin II Restricts Nitric Oxide and Peroxide Entry: Model of Ligand Control for the Design of a Stable Oxygen Carrier[†,‡]

Walleska De Jesús-Bonilla,[§,||] Yiping Jia,[||,⊥] Abdu I. Alayash,[*,⊥] and Juan López-Garriga[§]

Department of Chemistry, University of Puerto Rico, Mayagüez Campus, P.O. Box 9019, Mayagüez 00681-9019, Puerto Rico, and Laboratory of Biochemistry and Vascular Biology, Division of Hematology, Center for Biologics Evaluation and Research (CBER), Food and Drug Administration (FDA), Bethesda, Maryland 20892

Received February 20, 2007; Revised Manuscript Received July 6, 2007

ABSTRACT: Blood pressure elevation has been attributed in large part to the consumption of nitric oxide (NO) by extracellular hemoglobin (Hb) therapeutics following infusion in humans. We studied NO and hydrogen peroxide (H_2O_2) oxidative reaction kinetics of monomeric Hbs isolated from the clam *Lucina pectinata* to probe the effects of their distinctive heme pocket chemistries on ligand controls and heme oxidative stability. HbI (Phe43(CD1), Gln64(E7), Phe29(B10), and Phe68(E11)) reacted with high avidity with NO ($k'_{ox,NO} = 91\ \mu M^{-1}\ s^{-1}$), whereas HbII (Phe44(CD1), Gln65(E7), Tyr30(B10), and Phe69(E11)) reacted at a much slower rate ($k'_{ox,NO} = 2.8\ \mu M^{-1}\ s^{-1}$). However, replacing B10 (Phe) by Tyr in recombinant HbI (HbI PheB10Tyr) produced only a 2-fold reduction in the NO-induced oxidation rate ($k'_{ox,NO} = 49.9\ \mu M^{-1}\ s^{-1}$). Among the clam Hbs, HbII exhibited the fastest NO dissociation and the slowest NO association with ferrous iron. Autoxidation, H_2O_2-mediated ferryl iron (Fe^{IV}) formation, and the subsequent heme degradation kinetics were much slower in HbII and HbI PheB10Tyr when compared to those of HbI. The Tyr(B10) residue appears to afford a greater heme oxidative stability advantage toward H_2O_2, whereas the close proximity of this residue together with Gln(E7) to the heme iron contributes largely to the distal control of NO binding. Engineering of second-generation Hb-based oxygen therapeutics that are resistant to NO/H_2O_2-driven oxidation may ultimately require further optimization of the heme pocket architecture to limit heme exposure to solvent.

In spite of years of research and development efforts, clinical trials to date have revealed adverse effects resulting from infusions of Hb-based[1] oxygen carriers (HBOCs) (*1*−*3*). The NO-driven oxidation of the heme iron of the oxygenated forms of HBOCs and their elevated rates of spontaneous oxidation (autoxidation) are undesirable characteristics that clearly compromise the use of these Hbs in vivo. In addition to problems of oxidative toxicity, all HBOCs have demonstrated vasoconstrictive properties as a result of NO scavenging that result in imbalances in blood pressure control mechanisms in humans and animals (*4*). The successful commercial development of oxygen therapeutics "blood substitutes" has been hampered by the inability of current-generation oxygen therapeutics to carry oxygen effectively to tissues in part due to oxidation of their heme iron in vivo. The interference with NO, a blood vessel dilator and an important signaling molecule, leads to a sudden elevation in blood pressure among many other side effects (*2*, *4*).

Over the past decade there has been a concentrated effort in the use of protein engineering to reconstruct the heme pocket stereochemistry to optimize efficient oxygen transport, enhance heme stability, and minimize interference of cell-free Hb with the vascular system. Experimental hemoprotein prototypes such as sperm whale myoglobins (Mbs) have been used to investigate the effect of site-directed mutagenesis in and around the heme pocket to produce mutants with favorable ligand binding characteristics, which include moderate oxygen affinity and resistance to spontaneous, chemical (H_2O_2), and NO-driven oxidation. Generally, at the distal heme pocket, two residues have been shown to play a significant role in modulating ligand reactivity, and these are leucine (B10) and histidine (E7). The focus of current mutagenesis strategies is to alter electrostatic and steric interactions between the bound ligand and residues at the Leu29(B10), His64(E7), and Val68(E11) positions. It has been shown, for example, that large apolar residues (Leu, Phe, Trp) at the B10 and E11 positions inhibit NO-induced and spontaneous oxidation in both Mb and Hb by excluding oxidants and proton donors from the immediate vicinity of the bound ligand (*5*).

[†] This work was supported in part by funds from NIH-NIGMS/MBRS-Score-2 (Grant S06GM08103-34) and the National Science Foundation, Cellular Biology (Grant 0544250).

[‡] The findings and conclusions in this paper have not been formally disseminated by the Food and Drug Administration and should not be construed to represent any Agency determination or policy.

* To whom correspondence should be addressed. Phone: (301) 827-3813. Fax: (301) 435-4034. E-mail: abdu.alayash@fda.hhs.gov.

[§] University of Puerto Rico.

[||] These authors contributed equally to this work.

[⊥] Food and Drug Administration.

[1] Abbreviations: Hb, hemoglobin; Mb, myoglobin; HBOC, hemoglobin-based oxygen carrier; NO, nitric oxide; H_2O_2, hydrogen peroxide; DBBF, human hemoglobin cross-linked with bis(3,5-dibromosalicyl) fumarate.

10.1021/bi7003262 CCC: $37.00 © 2007 American Chemical Society
Published on Web 08/24/2007

The diversity of invertebrate Hbs at both the structural and the functional levels provides unique model systems to investigate ligand binding to the protein, specifically the role of a given heme pocket chemistry in determining these reactions. Protein control of ligand binding at both the proximal and distal ends is very much influenced by the local architecture.

In this study, we have investigated ligand interactions, particularly of NO and H_2O_2, with HbI and HbII from the sulfide-fixing clam *Lucina pectinata* and compared these reactions with those of human HbA_0, chemically cross-linked human Hb, and a recombinant *L. pectinata* HbI, in which Phe(B10) was replaced by Tyr(B10). *L. pectinata* inhabits the sulfide-rich mangroves of the west coast of Puerto Rico. The clam lives in a symbiotic relationship with a chemoautotrophic bacterium in a cycle by which the three acellular Hbs (HbI, HbII, and HbIII) found in the clam circulation deliver and transport oxygen and hydrogen sulfide (H_2S). As a result of H_2S oxidation, the bacteria use the chemical energy generated to fix carbon dioxide into carbohydrates (hexose). The first Hb (HbI) isolated by size exclusion chromatography transports H_2S and is a monomer at all concentrations. The other two hemoglobins, HbII and HbIII, are oxygen-reactive Hbs and are monomers at low concentrations, while at high concentration (~4 mM) HbII tends to form oligomers of more than four subunits, and HbIII tends to dimerize at ~1 mM. A mixture of HbII/HbIII of ~6 mM tends to form a tetramer (*6*). In the distal site of the heme pocket of the three Hbs is a glutamine (Gln64(E7)) instead of the classical histidine; the glutamine residue is also present in elephant and shark Mbs (*7*). The other surrounding amino acid residues are three phenylalanines (Phe43(CD1), Phe68 (E11), Phe29(B10)) for HbI, while HbII and HbIII have two phenylalanines (Phe44(CD1), Phe69-(E11)) and a tyrosine residue (Tyr30(B10)).

Among the three Hbs investigated here, both oxy and ferric forms of HbII reacted extremely slowly with NO and its metabolites. Additionally, this Hb oxidizes in air slowly and exhibits unusual stability toward H_2O_2 oxidation. Our kinetic and structural data suggest that the proximity of Tyr(B10) and Gln(E7) to the heme iron in HbII minimizes the exposure of its heme to solvent, thus maintaining oxidative stability and reducing reactivity toward NO.

MATERIALS AND METHODS

Human Hemoglobins. Human cross-linked Hb (DBBF) generated by the reaction of deoxy stroma-free Hb with bis-(3,5-dibromosalicyl) fumarate and having a single intratetrameric cross-link between α chains at 99Lys was a kind gift from the U.S. Army, Walter Reed Army Hospital. It is the noncommercial analogue of DCLHb, the same molecule produced by Baxter, and has been extensively evaluated as a blood substitute and a pressor agent in trauma patients (*8*). Triple sperm whale (SW) mutant Mb (L29F/H64Q/V68F) was a kind gift from Professor John Olson of Rice University (*9*). A highly purified human HbA_0 used in some experiments was a kind gift from Hemosol Inc., Canada.

Isolation and Purification of Clam Hemoglobins. Isolation of different types of Hbs from the clam was performed following the method reported by Pietri et al. (*10*) after some modifications. Briefly, a size exclusion chromatography column, HiLoad 26/60 Superdex 200 prep grade (ÄKTA FPLC, Amersham Bioscience, Piscataway, NJ), was used to initially isolate the proteins from blood samples. HbI was subsequently separated from the cysteine-rich protein by ion exchange chromatography using a DEAE Fast Flow 16/62 column (ÄKTA FPLC, Amersham Bioscience) in 25 mM NH_4HCO_3, pH 8.3. buffers. Both HbII and HbIII were purified further after the HbII/HbIII fraction was subjected to another ion exchange chromatography with a Hi Prep 16/10 Q FF column equilibrated with 10 mM triethanolamine/acetate buffer at pH 8.3 and eluted with a gradient of sodium chloride concentration from 0 to 180 mM. The high-level purity of Hb preparations was confirmed by using SDS−PAGE analysis. Hb solutions were reduced by adding sodium dithionite ($Na_2S_2O_4$) and eluted through a Sephadex G-25 gel column in 50 mM potassium phosphate buffer.

The recombinant protein (HbI PheB10Tyr) was prepared as described by León et al. (*11*). The large-scale expression process was performed in a 5 L BioFlo 3000 fermentor (New Brunswick) following a procedure by Collazo et al. (*12*) with slight modifications. The red-brown pellets were lysed by five cycles of sonication using 10 mL of Tris−EDTA buffer (10 mM Tris−HCl, 0.1 mM EDTA, pH 8.0) for every 50 mL of culture centrifuge. The purification was achieved in three steps. First, the lysate was added to a metal affinity resin (Talon, Invitrogen). The resin was then washed with a wash buffer (50 mM Na_2PO_4, 0.3 M NaCl, and 15 mM imidazole, pH 7.6). After the last wash, 15−20 mL (for each 5 mL of resin) of elution buffer (50 mM Na_2PO_4, 0.3 M NaCl, 150 mM imidazole, pH 7.6) was used to elute the protein. The imidazole and salts were removed with a High Trap desalting column, and the final purification was achieved by size exclusion chromatography with a Sephadex G-25 column using an ÄKTA FPLC system (Amersham Biosciences).

Ferric Hbs were prepared by treating the oxy form of each Hb with potassium ferricyanide followed by an ultrafiltration step using Amicon YM 10 membranes to remove unreacted ferricyanide. Multicomponent analysis based on extinction coefficients of oxy, ferric, and ferryl species were used to calculate Hb redox species as previously reported (*13*).

Oxygen and Carbon Monoxide Binding Studies. Oxygen equilibrium binding studies were carried out in the Hemox analyzer (TCS Scientific, New Hope, PA) as previously described (*14*) to obtain P_{50} values. An Applied Photophysics SF-17 microvolume stopped-flow instrument was used to measure oxygen dissociation kinetics from oxy-Hbs and CO binding to deoxy-Hbs as described previously (*14*). The oxygen binding kinetics were measured by flash photolysis using 10 ns YAG laser pulses (Quantel, France) that provide 160 mJ at 532 nm as described previously (*15*). A low-intensity light source (50 W quartz halogen lamp filtered at 436 nm) was used. The samples placed in 1 mm cuvettes were monitored at 436 nm, and kinetic curves were an average of at least three traces recorded on a LeCroy 9400 oscilloscope.

Autoxidation Experiments. Autoxidation kinetics of all Hbs were determined at 37 °C for 24 h following a procedure by Jia et al. (*14*) with slight modifications. Briefly, Hbs (~20 μM) were reduced to maximum levels of the oxy-Hb forms (~90−95%) prior to autoxidation experiments and were incubated in air-equilibrated 50 mM Chelex-treated phos-

phate buffer with or without the antioxidant enzymes, catalase (414 U/mL), and superoxide dismutase (4.6 U/mL). The absorbance spectra between 400 and 700 nm were recorded over time in a temperature-controlled photodiode array spectrophotometer (HP-8453). The oxy-Hb percentage changes due to the spontaneous oxidation of Hbs were plotted as a function of time. The autoxidation rate constants were obtained by nonlinear least-squares curve fitting employing single- or double-exponential equations using SigmaPlot software.

Hydrogen Peroxide Reaction Kinetics with Hemoglobins. The reaction of the ferric forms of Hbs with H_2O_2 was performed under pseudo-first-order conditions as described previously using an Applied Photophysics SF-17 microvolume stopped-flow spectrophotometer with a diode array detector at 25 °C (*16*, *17*). Ferric Hb solutions (20 μM) were diluted in 0.5 mM Tris buffer, pH 7.4, with a final concentration of 10 μM and rapidly mixed with H_2O_2 ranging in concentration from 1 to 10 mM. These data were fitted to either a single- or double-exponential function using the Marquardt−Levenberg fitting routine included in the Applied Photophysics software. The apparent rate constants were given by curve fitting of the time courses measured at 400 nm. The second-order rate constants were obtained from the H_2O_2 concentration dependence on the apparent rate constants.

A rapid-mixing stopped-flow method we previously developed was used to detect the heme degradation fluorescent products in Hb solutions (*18*). The reactions were carried out for different Hbs under pseudo-first-order conditions in an Applied Photophysics SF-17 microvolume stopped-flow spectrophotometer. Time courses were acquired between 500 and 1000 s at 25 °C, with excitation at 321 nm and emission at ≥360 nm. Oxy-Hb solutions were diluted in 50 mM sodium phosphate buffer, pH 7.4, with a final concentration of 20 μM. Fluorescent degradation products formed as a result of the reaction of the Hb with H_2O_2 were monitored using concentrations of H_2O_2 between 4 and 8 mM. The pseudo-first-order rate constants were obtained with a single-exponential or double-exponential function using a software fitting routine program. The peroxide concentration dependence of the apparent rate constant for the reaction of the oxy form of Hbs (10 μM) was determined as a function of the peroxide concentration (2−4 mM) in the stopped-flow spectrophotometer. The second-order rate constant for the formation of degradation products was obtained from the slope of the linear relationship of the observed pseudo-first-order rate constant versus [H_2O_2]. No degradation can be observed without H_2O_2 under our conditions and time frame.

Nitric Oxide Reaction Kinetics with Hemoglobins. The kinetics of NO oxidation of the oxy forms of Hbs also known as "NO dioxygenation" were measured in the stopped-flow spectrophotometer (*19*). Prior to the mixing of the reactants, NO stock solutions (∼2 mM) were prepared by washing the gas through a deoxygenated solution of 1 M NaOH before saturating with a deoxygenated 0.05 M bis-Tris buffer, pH 7.0, in a gastight serum bottle at room temperature. This stock solution was then transferred to a gastight syringe for appropriate dilutions with deoxygenated bis-Tris buffer. Solutions of air-equilibrated Hb were mixed against anaerobic solutions of NO, and the conversion of oxy-Hb to ferric Hb was monitored by absorbance changes at 420 nm. The value of the bimolecular rate constant for this reaction is known to be extremely large, on the order of 1×10^7 M^{-1} s^{-1}(*20*), so the concentration of NO after mixing was kept low (≤25 μM) to minimize loss of the reaction in the dead time of the instrument. Under these conditions, the rate of autoxidation reaction of NO with dissolved oxygen is negligible compared with the rate of reaction with ferrous Hb. The concentration of Hb in this experiment was kept at 0.5 μM to use a pseudo-first-order approximation (*5*). The kinetics of NO binding to deoxy-Hbs were also measured in the stopped-flow instrument. Hb solutions in deoxygenated buffer were prepared by adding about 0.1 mg/mL sodium dithionite immediately before the reaction to remove any trace amount of oxygen. The Hb samples were mixed with the NO solution, and the reaction was monitored for the disappearance of deoxy-Hb at 435 nm as described previously (*21*).

NO dissociation rate constants were measured following a procedure by Farres et al. (*22*). Briefly, the dissociation was achieved by reacting HbNO formed from preincubated deoxy-Hb and NO solution with 1 mM CO/10 mM sodium dithionite solution. The changes in absorption were monitored at 420 nm using an HP UV spectrophotometer, and the spectra were recorded every 10 min during the first 3 h and every 30 min for a second 3 h period. The exponential fit of the kinetic traces was obtained for three independent experiments. Reactions of the ferric forms of Hbs (15 μM in heme) after being mixed with various concentrations of NO were monitored at 420 nm in an oxygen-free environment in the stopped-flow instrument as previously described (*23*).

Mass Spectrometry Analysis. The analysis of intact HbI and HbII was performed in the nanospray mode on the QSTAR-XL (Applied Biosystems, Foster City, CA) coupled to an LC Packings capillary HPLC instrument (Dionex, Atlanta, GA). The samples were dissolved in 0.01% TFA/0.05% acetic acid prior to column injection. A gradient from 0% to 60% TFA (0.01%)/acetic acid (0.05%) and TFA (0.01%)/acetic acid (0.05%) in acetonitrile was used for protein or peptide separation using a C18 100 Å column (15 cm × 75 nm, Vydac, Hesperia, CA). The QSTAR mass analyzer was optimized with the nanosource and operated in positive TOF-MS mode utilizing the information-dependent acquisition (IDA) mode. The source parameters were adjusted with the following settings: declustering potential (DP) 60 V, focusing potential (FP) 250 V, second declustering potential (DP2) 15 V, collision energy (CE) 0 (rolling energy), collision-activated dissociation (CAD) gas pressure 7 psi, ion release decay (IRD) 6 V, IRD 80.3. Switch criteria were established for ions greater than 150.00 *m*/*z* and for ions smaller than 1800.00 *m*/*z* to evaluate the entire ion envelope of Hbs.

RESULTS

Chromatographically purified native and recombinant clam Hbs were further analyzed by mass spectrometry techniques to confirm their molecular masses. The total ion current (TIC) chromatograph shown in Figure 1A is for HbI, which demonstrates a uniform distribution of ions occurring between 45 and 50 min. The apex corresponds to an *m*/*z* ratio of 874.86 amu representing a +17 ion. The charge state envelope shown in Figure 1B for HbI demonstrates a full

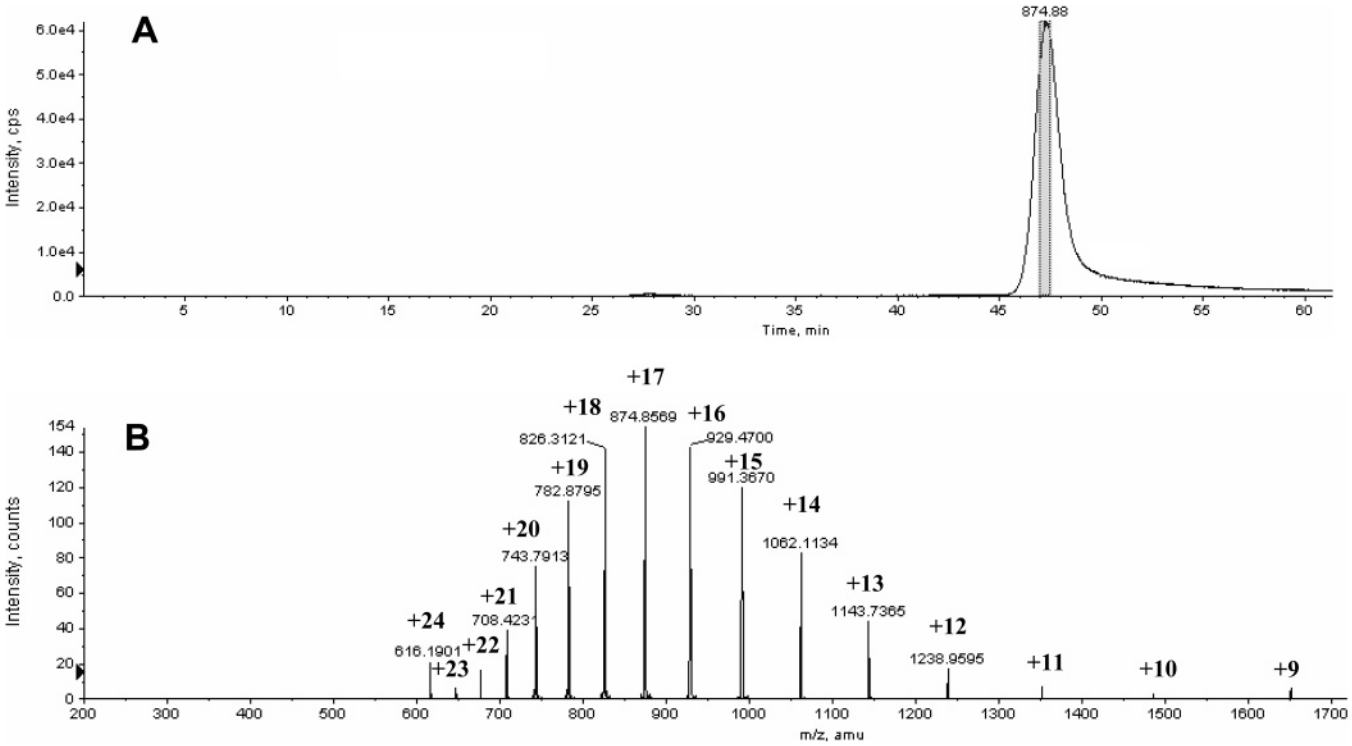

FIGURE 1: Charge state envelope and deconvoluted mass spectrum of HbI. (A) TIC of the HbI sample determined by a capillary HPLC instrument on a quadrupole-TOF mass spectrometer. The peak in the TIC at 47 min indicates an ion with an *m*/*z* ratio of 874.88 amu corresponding to a +17 ion. (B) The full scan mass spectrum of the peak from 46.99 to 47.54 min of the TIC showed a series of multiply charged ions for HbI as indicated from +9 to +24 ions that gave a deconvoluted mass of 14855.95 amu.

Table 1: Kinetic and Equilibrium Constants for Oxygen and Carbon Monoxide Reactions of Oxy/Deoxy Clam Hbs and Mutant Mb[a]

Hb	k'_{on,O_2}, $\mu M^{-1} s^{-1}$	k_{off,O_2}, s^{-1}	$1/K_{O_2}$, μM	P_{50}, mmHg	$k'_{on,CO}$, $\mu M^{-1} s^{-1}$
HbI	~200[b,c]	92.2 ± 3.8	0.31[d]	0.18[c]	6.94 ± 0.51
HbII	0.39[c]	0.146 ± 0.007	0.28[c]	0.13[c]	0.011 ± 0.001
HbI PheB10Tyr	6.8 ± 0.3	0.6 ± 0.02	0.09	0.05[b]	0.71 ± 0.012
Mb L29F/H64Q/V68F	16[e]	3[e]	0.19[e]	0.11[b]	10[e]

[a] Bimolecular rate constants k'_{on,O_2} and $k'_{on,CO}$ are the oxygen and CO binding constants. The oxygen dissociation rate constant is k_{off,O_2}, K_{O_2} is the oxygen equilibrium binding constant, and P_{50} is the partial pressure of oxygen at which Hb is 50% saturated. The values with errors are from this work. For experimental details see the Materials and Methods. [b] Estimated from k_{off} and $1/K_{O_2}$. [c] Kraus and Wittenberg (*6*). [d] Estimated from P_{50}. [e] Dou et al. (*42*).

range of ions from which the deconvoluted mass was calculated as 14855.95 amu, in good agreement with the value previously determined by the amino acid composition and from the cDNA-derived amino acid sequence (*6*, *24*). HbII demonstrates a similar yet less uniform pattern of ionization compared to HbI. The apex of the TIC occurring at 50 min elution time gave an ion envelope from which a mass of 16091.87 amu was obtained, consistent with the value determined previously by amino acid composition studies for this Hb (*6*). The recombinant HbI PheB10Tyr also exhibits a less uniform envelope of multiply charged ions from which the deconvoluted mass was close to the molecular weight of HbI. Crystallization and X-ray structure analysis of HbI and HbII were previously performed (*25*, *26*), and the structural disparities of the HbI and HbII heme pocket configurations were determined (discussed later).

Table 1 summarizes oxygen and carbon monoxide binding to clam Hbs compared to mutant Mb. Figure 2A shows time courses of the NO-induced oxidation of oxy-HbI in comparison to that obtained for HbII under the same stopped-flow conditions. These time courses were fitted well to a single-exponential expression with an offset. Plots of the pseudo-first-order rate constants, k_{obsd}, versus NO concentrations are linear as shown in Figure 2B for HbI, HbII, and the HbI PheB10Tyr mutant. Also shown in this figure is the plot derived for the reaction of human cross-liked Hb (DBBF), known for its vasoactivity in animals and humans because of its avid NO binding (*27*). The second-order rate constants of NO oxidation (k_{obsd}) for all Hbs are given in Table 2. A rate constant of 19 $\mu M^{-1} s^{-1}$ derived from these plots for DBBF is close to what we have previously reported (*28*) and is similar to rates reported by others for modified and unmodified Hbs (*21*) or recombinant Hbs (*29*) and falls within the reported range of wild-type Mb (*5*). As can be seen in Table 2, the rate derived for the clam HbI is approximately 4−5-fold faster than that of DBBF and 30 times higher in magnitude over that calculated for HbII. An intermediate value, however, for the rate constant for NO oxidation of the mutant HbI PheB10Tyr was obtained among the clam Hbs. Furthermore, all oxy-Hbs exhibited rate constants for NO-induced oxidation very similar to that of NO binding to their deoxy forms as reported in Table 2. The replacement of NO by CO allowed for the NO dissociation rate to be calculated for these deoxy-Hbs bound

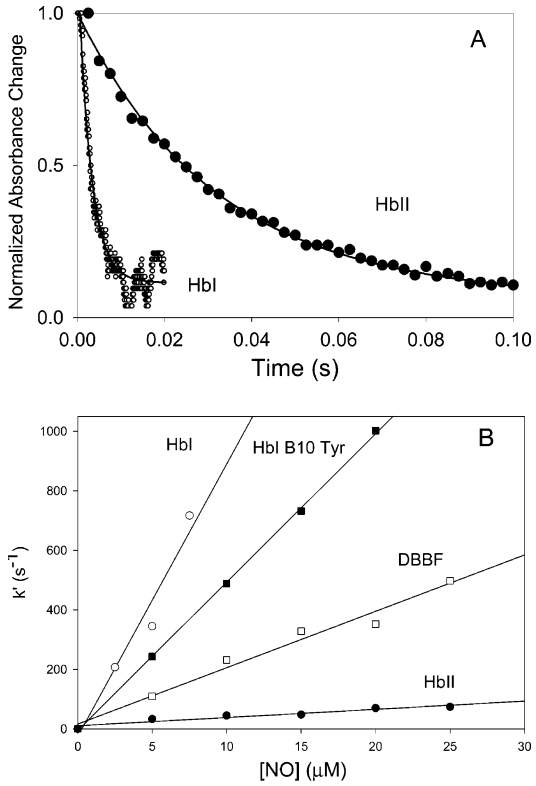

FIGURE 2: Stopped-flow kinetics of NO-induced oxidation of DBBF and clam Hbs. (A) Normalized time courses for the reactions of 5 μM NO and 0.5 μM (heme, after mixing) HbI and HbII. The solid lines are the nonlinear least-square fits to the exponential equation. (B) Observed first-order rate constants versus NO concentrations for the reactions of NO with 0.5 μM oxy-Hbs. The bimolecular rate constants of NO-induced oxidation reaction of DBBF and the clam Hbs are reported in Table 2.

with NO as shown in Figure 3. The rate constant ($k_{off,\ NO}$) for human Hb, DBBF, is similar in value to those reported for native Hb and is significantly lower than the calculated value for the clam Hbs. The rate of NO dissociation from HbII is 1.5-fold higher than that of HbI and its recombinant derivative HbI PheB10Tyr (Table 2). Moreover, the equilibrium binding constants of NO and these deoxy-Hbs were calculated and are reported in Table 2. Reaction of NO with the ferric forms of unmodified and chemically cross-linked Hbs has been reported to be a sensitive probe for heme pocket alterations irrespective of their oxygen affinities (*23*). Figure 4 shows the time course of the initial events accompanying the mixing of the ferric forms of HbI and HbII with NO. In Table 2, the rate constants for the combination of NO with ferric HbI and ferric HbII are reported and compared to those obtained for both recombinant clam Hb and DBBF. HbII again shows a much slower binding rate to the ferric iron than the rates calculated for HbI and the HbI PheB10Tyr mutant included in this study under the same experimental conditions. Furthermore, in a much slower process driven by an excess amount of NO the ferric hemes of Hbs become reduced (*23*). The reductive nitrosylation of the ferric forms of both HbI and HbII was 2-fold faster than that measured for metDBBF (data not shown).

The left panel in Figure 5 shows typical spectra taken at the beginning of the autoxidation experiments of HbI, HbII, and HbI PheB10Tyr and at the end of the first 6 h of incubation. The right panel presents typical autoxidation time courses of the three Hbs derived from continued monitoring of spectral changes throughout the incubation time. The calculated rates derived from similar autoxidation experiments carried out on DBBF and other proteins are included in Table 3. The DBBF autoxidation rate was reduced by approximately 30−40% when antioxidant enzymes such as superoxide dismutase (SOD) and catalase were added to the protein solution prior to the start of the autoxidation experiment, consistent with earlier reports, and confirms the buildup of oxygen free radicals during the autoxidation process (*30*, *31*). The kinetic rate constants for the clam Hbs were several-fold lower than that of DBBF (e.g., 9−11-fold lower in the case of HbII and HbI PheB10Tyr, respectively). There was little or no change in those rates when antioxidant enzymes (SOD and catalase) were added (Table 3). Long-term stability studies in the absence of antioxidant enzymes showed that at the end of 24h incubation time period there was 22% and 41% ferric Hb present in HbI PheB10Tyr and HbII solutions, respectively. However, very little ferric HbI was found, but almost 40% of the total heme was instead transformed to other oxidized denatured products such as hemichromes within the first 6 h of incubation. The susceptibility of HbI to oxidative modification and heme degradation was also confirmed by its high reaction rate with H_2O_2 and subsequent fluorescent heme degradation product formation as evident in Table 3 when compared to those of other proteins.

DISCUSSION

One of the most widely accepted interpretations of blood pressure imbalances in patients receiving Hb-based transfusion therapy is the inactivation of NO by extracellular Hb. Site-directed mutations at His(E7), Leu(B10), and Val(E11) mostly carried out in Mb prototypes have generally been replaced by large apolar residues to restrict NO entry to the heme pocket. Substitution of His(E7) with Gln, the only other residue able to establish a H-bond with oxygen, has been the target of oxygen affinity lowering effects. Replacing Val68(E11) with Phe or Leu29(B10) with larger Phe, Trp, and Tyr residues causes significant decreases in NO-induced oxidation rates in Mb and Hb. A series of genetically modified Hbs containing Phe, Gln, and Trp mutations in the α and β subunits produced similar results. However, heme stability in some of these mutants is often compromised as a result of distal pocket alterations. Mb mutants, for example, in which His64 was replaced with Gln singularly or in combination with Phe(B10) showed efficient pseudoperoxidase activity and favorable NO and oxygen binding characteristics but an enhanced heme loss and breakdown (*32*). The effects of some of these recombinant Hbs were tested in several animal models of exchange transfusion and showed improved blood pressure control as well as improvement in blood flow and tissue oxygenation (*33*, *34*). However, clinical development of these new recombinant Hbs with heme pocket alterations were recently abandoned (*35*).

The success of intracellular oxygen carriers in animals in large part is due to the packaging of these molecules with reductants and allosteric modifiers of the Hb affinity within red blood cells. The challenges of preparing cell-free Hbs that achieve all the advantages of natural intracellular oxygen carriers have been overcome in some species by the evolutionary development of the high molecular weight heme

Table 2: Kinetic and Equilibrium Constants for NO Reaction with the Oxy, Deoxy, and Met Forms of Clam Hbs, Human Cross-Linked Hb, and Mutant Mb[a]

Hb	$k'_{ox,NO}$, $\mu M^{-1} s^{-1}$	$k'_{NO}(Fe^{2+})$, $\mu M^{-1} s^{-1}$	$k_{off,NO}$, $10^{-4} s^{-1}$	K_{NO}, $10^4 \mu M^{-1}$	$k'_{NO}(Fe^{3+})$, $\mu M^{-1} s^{-1}$
DBBF	19.0 ± 1.4	20.9 ± 2.7	1.2 ± 0.14	17.4	0.019 ± 0.0021
HbI	~91.6	~109.1	4.0 ± 0.37	~27.3	3.85 ± 0.70
HbII	2.8 ± 0.4	2.4 ± 0.5	7.1 ± 0.53	0.33	0.66 ± 0.04
HbI PheB10Tyr	49.9 ± 0.6	52.3 ± 4.2	5.6 ± 0.26	9.3	3.09 ± 0.38
Mb L29F/H64Q/V68F	13[b]	10[b]	1.2[b]	8.3	4.10 ± 0.28

[a] $k'_{ox,NO}$ is the bimolecular rate constant for NO-induced oxidation of oxy-Hb. $k'_{NO}(Fe^{2+})$ and $k'_{NO}(Fe^{3+})$ are the bimolecular rate constants for NO binding to deoxy-Hb and met-Hb, respectively. The NO dissociation rate constant is $k_{off,NO}$. K_{NO} is the calculated equilibrium binding constant of NO and deoxy-Hb. For experimental details see Materials and Methods. [b] Dou et al. (*42*).

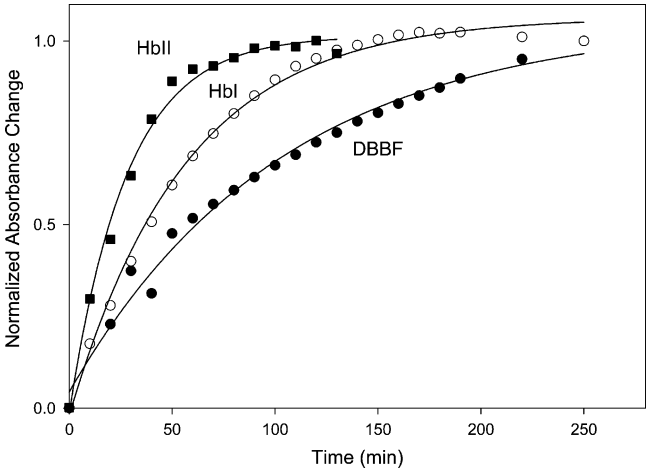

FIGURE 3: NO dissociation time courses from DBBF and clam Hbs. Deoxygenated Hbs (5 μM) were mixed in an equal molar ratio with NO and then incubated with 1 mM CO and 10 mM sodium dithionite in 100 mM sodium phosphate buffer, pH 7.4, in sealed cuvettes. NO dissociation was measured at 420 nm in a spectrophotometer. The absorbance changes of various Hbs were normalized to 1 at the maximum absorbance for data comparison. The solid lines are the nonlinear least-square fits to the single-exponential equation.

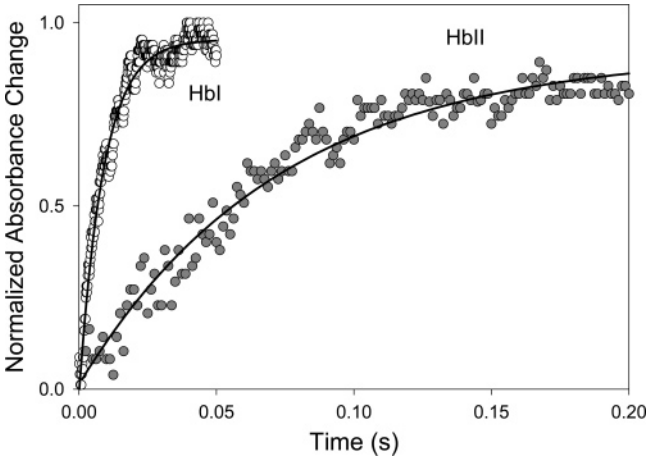

FIGURE 4: Reaction kinetics of ferric clam Hbs with NO. Stopped-flow time courses of reactions between 0.5 μM (after mixing) ferric HbI and HbII and 15 μM NO solution monitored at 420 nm in 50 mM sodium phosphate buffer at pH 7.4 and 20 °C. The solid lines are the nonlinear least-square fits to the exponential equation.

proteins, erythrocruorins, that serve as oxygen carriers in marine and terrestrial worms. The high molecular weight polymeric *Lubricous terrestris* Hb is another successful example in which oxygen-carrying capabilities are combined with unusually stable heme pockets with well-controlled oxidation reactions in an extracellular environment (*36*).

The mollusk *L. pectinata* lives in sulfide-rich mangroves of Puerto Rico, and it exists in a symbiotic relationship with bacteria that live in its gills in which both sulfur and oxygen are exchanged in return for carbohydrate nutritional supplies. Both HbI and HbII isolated from the clam bind oxygen noncooperatively with high affinity, even higher than that observed for sperm whale Mb (Table 1). Resonance Raman, X-ray crystal structure, and functional studies showed that both Gln(E7) and Phe(B10) contribute toward stabilizing bound ligands and that the flexibility of the HbI distal site is directed mainly by Gln(E7), which controls ligand reactivity. Stabilizing heme-bound oxygen by the Tyr(B10) residue in HbII as well as in other nonvertebrate Hbs, such as those from *Mycobacterium tuberculosis*, *Ascaris suum*, and bacterial flavohemoglobin has been demonstrated recently (*10*, *37*, *38*). It has also been shown that the flexibility of the flavohemoglobin heme pocket allows the movement of both Gln(E7) and Tyr(B10) closer to the heme to accommodate both oxygen and NO molecules simultaneously to function as NO dioxygenase and to provide protection against NO and related reactive species and adopt a peroxidase-like structure to perform its function (*39*).

Clams and other water-breathing organisms are regularly and naturally exposed to NO, H_2S, and CO, for these gases occur normally in seawater. In general, the concentration of NO particularly in seawater is on the order of $\sim 2 \times 10^{-12}$ M. It is tempting to speculate that the coexistence of cysteine-rich proteins and sulfur/NO-carrying proteins in the clam blood together with the strategic positioning of a few amino acids in the heme pocket in HbII may have been possibly involved in a regulatory mechanism against nitrosative stress (*40*). Regardless of the precise role of HbII in NO physiology in the *L. pectinata* clam, the unusually well controlled NO entry in the heme pocket, on the basis of the kinetic and structural data presented in our work (see below), may represent a model for the design of oxidatively stable oxygen therapeutics with little or no vasoactivity.

The heme pocket of HbI mimics the triple mutant of sperm whale Mb (L29F/H64Q/V68F) that has a similar oxygen affinity but higher association and dissociation rate constants (Table 1). Engineering of these three residues in sperm whale Mb produced 7-fold lower sulfide affinity to Mb compared to that of *L. pectinata* HbI. Comparison of the solution and crystal structure of the triple mutant with that of HbI from the clam showed that the latter has a significantly larger ligand binding site than that found in Mb mutants, which should facilitate the binding of a large H_2S ligand. Additionally, it has been suggested that changes in the orientation of Phe29(B10) and Phe68(E11) and the decrease in the size of

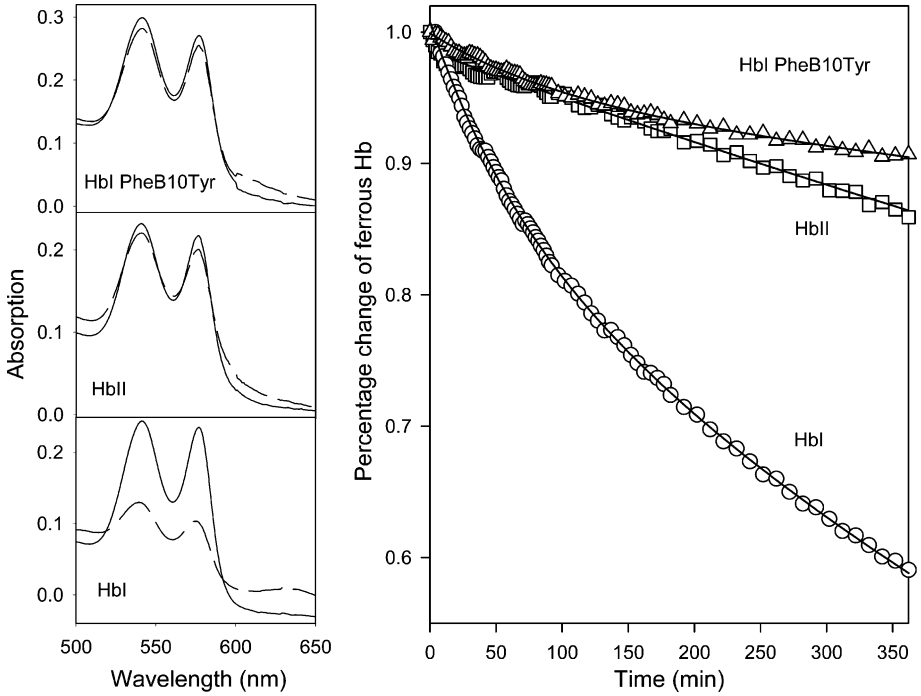

FIGURE 5: Spectral changes during autoxidation of clam Hbs and time courses of the decay of the oxy form of Hbs as a function of time. Spectral changes were measured during the autoxidation of 20 μM Hb in air-equilibrated 50 mM phosphate buffer, pH 7.4, at 37 °C in a spectrophotometer. Spectra measured at time 0 (solid line) and after 6 h of incubation (dashed line) are shown for each Hb in the left panel. Time courses of changes in the percentages of oxy-Hb derived from the spectral changes during the autoxidation experiments are shown in the right panel.

Table 3: Autoxidation and Peroxide-Mediated Oxidation Reaction Rate Constants for the Clam and Human Cross-Linked Hbs[a]

Hb	k_{autox}, h^{-1}	k_{autox}(+SOD/cat), h^{-1}	$k_{H_2O_2,ox}$, $M^{-1}\,s^{-1}$	$k_{H_2O_2,heme\ degradation}$, $M^{-1}\,s^{-1}$
DBBF	0.09 ± 0.001	0.05 ± 0.001	120.5 ± 5.6	8.0 ± 1.6
HbI	0.055 ± 0.008	0.058 ± 0.001	403.2 ± 2.7	37 ± 6.3
HbII	0.01 ± 0.0002	0.01 ± 0.0002	64.0 ± 2.3	1.1 ± 0.6
HbI PheB10Tyr	0.008 ± 0.001	0.005 ± 0.0001	52.0 ± 4.7	1.2 ± 0.04

[a] k_{autox} is the initial autoxidation rate constant for the spontaneous oxidation of Hbs measured at 37 °C in the presence or absence of antioxidant enzymes (SOD and catalase). $k_{H_2O_2,ox}$ is the oxidation reaction rate constant of ferric Hb by H_2O_2 measured at 400 nm. $k_{H_2O_2,heme\ degradation}$ is the rate of fluorescent heme degradation product formation induced by H_2O_2. For experimental details see Materials and Methods.

the distal pocket in the mutant may also have accounted for these differences (*41*).

We report a NO-induced oxidation rate for the triple mutant of 21.5 $\mu M^{-1}\ s^{-1}$, similar in magnitude to that reported originally by Olson and collaborators (*42*) and far less than the value of 91 $\mu M^{-1}\ s^{-1}$ calculated for HbI (Table 2). In the case of HbI, this unusually high rate for NO-induced oxidation is matched by much higher association and dissociation rate constants.

It has been suggested that the NO-induced oxidation is favored in those hemoproteins that have larger oxygen association rate constants and smaller oxygen dissociation rate constants as the $Fe^{2+}-O_2$ intermediate is required for this reaction (*42*). It is not surprising therefore that the NO-induced oxidation rate derived for HbII is extremely low compared to that derived for all hemoproteins including DBBF, a well-known vasoactive Hb with extremely low oxygen association and dissociation kinetics. It has been previously shown that the introduction of appropriate polar residues at both the B10 and E7 positions has induced a substantial reduction in the reaction of NO in the case of recombinant Mb and Hb (*9*). Introduction of Tyr in the B10 position and Gln in the E7 position in the human Hb α and β subunits (Hb$\alpha\beta$ YQ) produced a mutant with a very low reactivity toward NO. The crystallographic structure of this mutant Hb in particular provided some stereochemical basis for the reduced reactivity. Our data, however, showed that the introduction of Tyr(B10) in the heme pocket of recombinant HbI in combination with Gln did not completely reverse NO-induced oxidation of this Hb (Table 2).

The comparison of the functional and structural consequences of Tyr(B10) and Gln(E7) on the ligand binding dynamics in two invertebrate Hbs, *Ascaris suum* and *L. pectinata* HbI and HbII, has been carried out to determine the contribution of the heme pocket architecture to the dynamic control of these reactions. The hydrogen-bonding network that includes the Gln(E7), Tyr(B10), and oxygen bound to the heme results in a tight gage for the oxygen in *Ascaris* Hb. This explains why *A. suum* Hb has one of the highest oxygen affinities known, while *L. pectinata* HbI has an affinity comparable to that of Mb, even though both of the clam Hbs contain the Tyr(B10) and Gln(E7) motif and display very low oxygen off rates (*43*).

Unlike NO binding to the oxy-Hb, the kinetics of reaction of this ligand with the ferric iron are controlled by a completely different stereochemistry. In the case of ferric

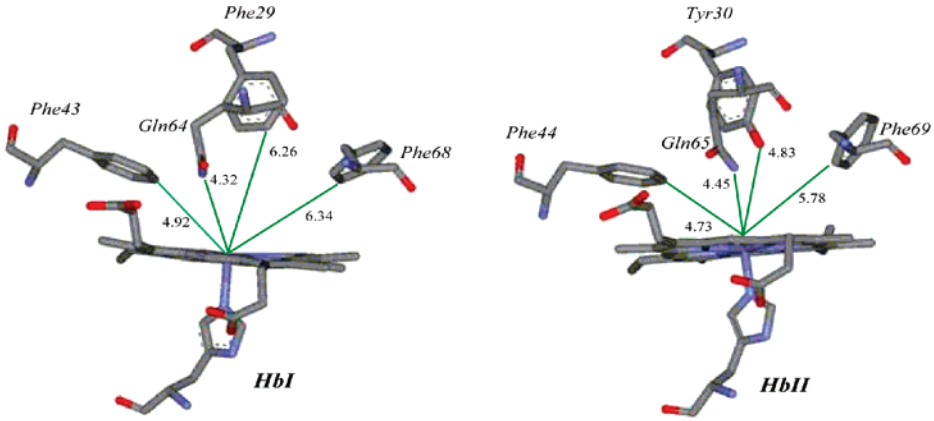

FIGURE 6: Stereo diagrams of the orientations of the distal residues of *L. pectinata*'s HbII and HbI. The distances (Å) from the residues to the heme Fe atom were calculated from the C-ζ in Phe, the N of the amide in the glutamine, and the oxygen in the tyrosine.

Mb, water coordinates with the iron atom and as a result ligand binding is limited in part by the strength of the $Fe^{3+}-OH_2$ bond (*44*, *45*). In wild-type ferric Mb, the rate constants for NO binding were found to be ~100 times smaller than the rate constants for NO binding and oxidation of corresponding oxygenated protein. However, aromatic substitutions at the 29(B10) and 68(E11) positions caused a much smaller decrease in $k_{NO}(Fe^{3+})$ than those observed for $k_{ox,NO}$ and $k_{NO}(Fe^{2+})$. The rate for NO binding to the ferric forms of HbI and its mutant were approximately 23 and 16 times smaller than the respective oxidation of their ferrous iron by NO. The NO binding to the ferric HbII is again the lowest among the clam Hbs and like that of the triple-mutant Mb only 4−5 times smaller in magnitude than the rates of the respective reactivity of their ferrous iron with NO.

The Phe(B10) substitution of the Leu residue in mutant Mb was shown to decrease the rate of autoxidation by at least 10-fold compared to the rate of autoxidation of the native Mb. The large benzyl side chain inhibits autoxidation reactions by both stabilizing bound oxygen and filling the space adjacent to the bound oxygen. However, our data show that the presence of Tyr(B10) in HbII and in HbI PheB10Tyr appear to afford a more stable oxygen adduct in the oxygenated form of these Hbs than does Phe(B10) in HbI. The contribution of Tyr(B10) toward the stability of the heme pocket as in the case of HbII and HbI PheB10Tyr in the face of H_2O_2 attack has recently been shown to be in part due to presence of hydrogen bonding between the ferryl moiety and the heme pocket amino acids including Tyr(B10), which ultimately enhance the removal of H_2O_2 by the peroxidative cycle (*17*).

We have recently examined the dynamical features of HbI, Mb, and the L29F/H64Q/V68F triple mutant of SW Mb, both unliganded and bound to H_2S, including rigid body motion, relative orientation of the heme prosthetic group within the HbI, hydrogen bond formation between the heme propionate groups and nearby amino acid residues, and changes in the distal cavity volume. These studies revealed the existence of a much greater heme freedom in HbI than in SW Mb. The active-site residues Gln64(E7), Phe43(CD1), and His93(F8) are also shown to be more flexible in unligated HbI than in the L29F/H64Q/V68F mutant and SW Mb (*26*). On the basis of our recent capillary crystallization and molecular solution studies of HbII (*25*), we calculated using the PDB the distances of the key residues Gln65(E7), Tyr30(B10), Phe44(CD1), and Phe69(E11) in the hydrophobic distal cavity from the heme Fe atom to be 4.45, 4.83, 4.73, and 5.78 Å, respectively (HbII structure PDB ID code 2OLP). Accordingly, this heme pocket is much smaller than that of the HbI distal center containing Gln64(E7), Phe29(B10), Phe43(CD1), and Phe68(E11), for which the calculated distances from the heme Fe atom are 4.32, 6.26, 4.92, and 6.34 Å, respectively (Figure 6). Furthermore, the heme pocket in chain B of the HbII dimer is slightly more collapsed than in chain A, as shown by the shorter distance between the O of the distal tyrosine and the iron atom (4.81 Å in chain A and 4.56 Å in chain B) and the volume size of the heme cavity (911.6 $Å^3$ in chain A and 834.9 $Å^3$ in chain B). These distances suggest that the architecture of the HbII heme pocket is slightly narrower than that of Hb I.

In summary, we show here that the two Hbs isolated from the blood of the clam *L. pectinata* with similar distal pocket amino acid compositions, with the exception of one amino acid at the B10 position (i.e., Tyr in HbII vs Phe in HbI), show remarkable differences in their reaction with ligands, particularly NO. However, re-engineering of the HbI heme pocket to include Tyr(B10) did not suppress the NO-induced oxidation activity of mutant Hb to the same level as that of HbII. The residue Tyr(B10) appears to provide overall better resistance to oxidative insult by H_2O_2 than is the case with HbI. Our calculation of the proximity of this residue together with Gln(E7) to the heme iron confirms the reduced solvent accessibility of the heme group, which subsequently leads to reduced NO gating to the heme pocket.

ACKNOWLEDGMENT

We thank Professor John Olson of Rice University for sperm whale myoglobin mutant proteins and helpful discussion regarding this work. We also thank Dr. Paul W. Buehler of the Food and Drug Administration for carefully reading the manuscript.

REFERENCES

1. Vandegriff, K. D. (2000) Haemoglobin-based oxygen carriers, *Expert Opin. Invest. Drugs 9*, 1967−1984.
2. Mackenzie, C. F., and Bucci, C. (2004) Artificial oxygen carriers for trauma: myth or reality, *Hosp. Med. 65*, 582−588.
3. Stowell, C. P., Levin, J., Spiess, B. D., and Winslow, R. M. (2001) Progress in the development of RBC substitutes, *Transfusion 41*, 287−299.

4. Alayash, A. I. (2004) Oxygen therapeutics: can we tame haemoglobin, *Nat. Rev. Drug Discovery 3*, 152−159.
5. Eich, R. F., Li, T., Lemon, D. D., Doherty, D. H., Curry, S. R., Aitken, J. F., Mathews, A. J., Johnson, K. A., Smith, R. D., Phillips, G. N., Jr., and Olson, J. S. (1996) Mechanism of NO-induced oxidation of myoglobin and hemoglobin, *Biochemistry 35*, 6976−6983.
6. Kraus, D. W., and Wittenberg, J. B. (1990) Hemoglobins of the Lucina pectinata/bacteria symbiosis. I. Molecular properties, kinetics and equilibria of reactions with ligands, *J. Biol. Chem. 265*, 16043−16053.
7. Zhao, X., Vyas, K., Nguyen, B. D., Rajarathnam, K., La Mar, G. N., Li, T., Phillips, G. N., Jr., Eich, R. F., Olson, J. S., and Ling, J., et al. (1995) A double mutant of sperm whale myoglobin mimics the structure and function of elephant myoglobin, *J. Biol. Chem. 270*, 20763−20774.
8. D'Agnillo, F., and Alayash, A. I. (2000) Site-specific modifications and toxicity of blood substitutes. The case of diaspirin cross-linked hemoglobin, *Adv. Drug Delivery Rev. 40*, 199−212.
9. Olson, J. S., Eich, R. F., Smith, L. P., Warren, J. J., and Knowles, B. C. (1997) Protein engineering strategies for designing more stable hemoglobin-based blood substitutes, *Artif. Cells, Blood Substitutes, Immobilization Biotechnol. 25*, 227−241.
10. Pietri, R., Granell, L., Cruz, A., De Jesus, W., Lewis, A., Leon, R., Cadilla, C. L., and Garriga, J. L. (2005) Tyrosine B10 and heme-ligand interactions of Lucina pectinata hemoglobin II: control of heme reactivity, *Biochim. Biophys. Acta 1747*, 195−203.
11. Leon, R. G., Munier-Lehmann, H., Barzu, O., Baudin-Creuza, V., Pietri, R., Lopez-Garriga, J., and Cadilla, C. L. (2004) High-level production of recombinant sulfide-reactive hemoglobin I from Lucina pectinata in Escherichia coli. High yields of fully functional holoprotein synthesis in the BLi5 E. coli strain, *Protein Expression Purif. 38*, 184−195.
12. Collazo, E., Pietri, R., De Jesus, W., Ramos, C., Del Toro, A., Leon, R. G., Cadilla, C. L., and Lopez-Garriga, J. (2004) Functional characterization of the purified holo form of hemoglobin I from Lucina pectinata overexpressed in Escherichia coli, *Protein J. 23*, 239−245.
13. Winterbourn, C. C. (1985) in *CRC Handbook of Methods for Oxygen Radical Research* (Greenwald, R. A., Ed.) pp 137−141, CRC Press, Boca Raton, FL.
14. Jia, Y., Wood, F., Menu, P., Faivre, B., Caron, A., and Alayash, A. I. (2004) Oxygen binding and oxidation reactions of human hemoglobin conjugated to carboxylate dextran, *Biochim. Biophys. Acta 1672*, 164−173.
15. Dewilde, S., Kiger, L., Burmester, T., Hankeln, T., Baudin-Creuza, V., Aerts, T., Marden, M. C., Caubergs, R., and Moens, L. (2001) Biochemical characterization and ligand binding properties of neuroglobin, a novel member of the globin family, *J. Biol. Chem. 276*, 38949−38955.
16. Nagababu, E., Ramasamy, S., Rifkind, J. M., Jia, Y., and Alayash, A. I. (2002) Site-specific cross-linking of human and bovine hemoglobins differentially alters oxygen binding and redox side reactions producing rhombic heme and heme degradation, *Biochemistry 41*, 7407−7415.
17. De Jesus-Bonilla, W., Cruz, A., Lewis, A., Cerda, J., Bacelo, D. E., Cadilla, C. L., and Lopez-Garriga, J. (2006) Hydrogen-bonding conformations of tyrosine B10 tailor the hemeprotein reactivity of ferryl species, *J. Biol. Inorg. Chem. 11*, 334−342.
18. Jia, Y., and Alayash, A. I. (2002) Stopped-flow fluorescence method for the detection of heme degradation products in solutions of chemically modified hemoglobins and peroxide, *Anal. Biochem. 308*, 186−188.
19. Alayash, A. I., Summers, A. G., Wood, F., and Jia, Y. (2001) Effects of glutaraldehyde polymerization on oxygen transport and redox properties of bovine hemoglobin, *Arch. Biochem. Biophys. 391*, 225−234.
20. Olson, J. S., Foley, E. W., Rogge, C., Tsai, A. L., Doyle, M. P., and Lemon, D. D. (2004) No scavenging and the hypertensive effect of hemoglobin-based blood substitutes, *Free Radical Biol. Med. 36*, 685−697.
21. Vandegriff, K. D., Bellelli, A., Samaja, M., Malavalli, A., Brunori, M., and Winslow, R. M. (2004) Kinetics of NO and O2 binding to a maleimide poly(ethylene glycol)-conjugated human haemoglobin, *Biochem. J. 382*, 183−189.
22. Farres, J., Rechsteiner, M. P., Herold, S., Frey, A. D., and Kallio, P. T. (2005) Ligand binding properties of bacterial hemoglobins and flavohemoglobins, *Biochemistry 44*, 4125−4134.
23. Alayash, A. I., Fratantoni, J. C., Bonaventura, C., Bonaventura, J., and Cashon, R. E. (1993) Nitric oxide binding to human ferrihemoglobins cross-linked between either alpha or beta subunits, *Arch. Biochem. Biophys. 303*, 332−338.
24. Antommattei-Perez, F. M., Rosado-Ruiz, T., Cadilla, C. L., and Lopez-Garriga, J. (1999) The cDNA-derived amino acid sequence of hemoglobin I from Lucina pectinata, *J. Protein Chem. 18*, 831−836.
25. Gavira, J. A., de Jesus, W., Camara-Artigas, A., Lopez-Garriga, J., and Garcia-Ruiz, J. M. (2006) Capillary crystallization and molecular-replacement solution of haemoglobin II from the clam Lucina pectinata, *Acta Crystallogr., Sect. F: Struct. Biol. Cryst. Commun. 62*, 196−199.
26. Fernandez-Alberti, S., Bacelo, D. E., Binning, R. C., Jr., Echave, J., Chergui, M., and Lopez-Garriga, J. (2006) Sulfide-binding hemoglobins: Effects of mutations on active-site flexibility, *Biophys. J. 91*, 1698−1709.
27. Abassi, Z., Kotob, S., Pieruzzi, F., Abouassali, M., Keiser, H. R., Fratantoni, J. C., and Alayash, A. I. (1997) Effects of polymerization on the hypertensive action of diaspirin cross-linked hemoglobin in rats, *J. Lab. Clin. Med. 129*, 603−610.
28. Rogers, M. S., Ryan, B. B., Cashon, R. E., and Alayash, A. I. (1995) Effects of polymerization on the oxygen carrying and redox properties of diaspirin cross-linked hemoglobin, *Biochim. Biophys. Acta 1248*, 135−142.
29. Doyle, M. P., Apostol, I., and Kerwin, B. A. (1999) Glutaraldehyde modification of recombinant human hemoglobin alters its hemodynamic properties, *J. Biol. Chem. 274*, 2583−2591.
30. Yang, T., and Olsen, K. W. (1994) Enzymatic protection from autoxidation for crosslinked hemoglobins, *Artif. Cells, Blood Substitutes, Immobilization Biotechnol. 22*, 709−717.
31. Watkins, J. A., Kawanishi, S., and Caughey, W. S. (1985) Autoxidation reactions of hemoglobin A free from other red cell components: a minimal mechanism, *Biochem. Biophys. Res. Commun. 132*, 742−748.
32. Alayash, A. I., Ryan, B. A., Eich, R. F., Olson, J. S., and Cashon, R. E. (1999) Reactions of sperm whale myoglobin with hydrogen peroxide. Effects of distal pocket mutations on the formation and stability of the ferryl intermediate, *J. Biol. Chem. 274*, 2029−2037.
33. Doherty, D. H., Doyle, M. P., Curry, S. R., Vali, R. J., Fattor, T. J., Olson, J. S., and Lemon, D. D. (1998) Rate of reaction with nitric oxide determines the hypertensive effect of cell-free hemoglobin, *Nat. Biotechnol. 16*, 672−676.
34. Raat, N. J., Liu, J. F., Doyle, M. P., Burhop, K. E., Klein, J., and Ince, C. (2005) Effects of recombinant-hemoglobin solutions rHb2.0 and rHb1.1 on blood pressure, intestinal blood flow, and gut oxygenation in a rat model of hemorrhagic shock, *J. Lab. Clin. Med. 145*, 21−32.
35. Winslow, R. M. (2006) Current status of oxygen carriers ('blood substitutes'), *Vox Sang 91*, 102−110.
36. Hirsch, R. E., Jelicks, L. A., Wittenberg, B. A., Kaul, D. K., Shear, H. L., and Harrington, J. P. (1997) A first evaluation of the natural high molecular weight polymeric Lumbricus terrestris hemoglobin as an oxygen carrier, *Artif. Cells, Blood Substitutes, Immobilization Biotechnol. 25*, 429−444.
37. Yeh, S. R., Couture, M., Ouellet, Y., Guertin, M., and Rousseau, D. L. (2000) A cooperative oxygen binding hemoglobin from Mycobacterium tuberculosis. Stabilization of heme ligands by a distal tyrosine residue, *J. Biol. Chem. 275*, 1679−1684.
38. Yang, J., Kloek, A. P., Goldberg, D. E., and Mathews, F. S. (1995) The structure of Ascaris hemoglobin domain I at 2.2 A resolution: molecular features of oxygen avidity, *Proc. Natl. Acad. Sci. U.S.A. 92*, 4224−4228.
39. Mukai, M., Mills, C. E., Poole, R. K., and Yeh, S. R. (2001) Flavohemoglobin, a globin with a peroxidase-like catalytic site, *J. Biol. Chem. 276*, 7272−7277.
40. Gow, A. J., Payson, A. P., and Bonaventura, J. (2005) Invertebrate hemoglobins and nitric oxide: how heme pocket structure controls reactivity, *J. Inorg. Biochem. 99*, 903−911.
41. Scott, E. E., Gibson, Q. H., and Olson, J. S. (2001) Mapping the pathways for O2 entry into and exit from myoglobin, *J. Biol. Chem. 276*, 5177−5188.
42. Dou, Y., Maillett, D. H., Eich, R. F., and Olson, J. S. (2002) Myoglobin as a model system for designing heme protein based blood substitutes, *Biophys. Chem. 98*, 127−148.
43. Peterson, E. S., Huang, S., Wang, J., Miller, L. M., Vidugiris, G., Kloek, A. P., Goldberg, D. E., Chance, M. R., Wittenberg, J. B.,

and Friedman, J. M. (1997) A comparison of functional and structural consequences of the tyrosine B10 and glutamine E7 motifs in two invertebrate hemoglobins (Ascaris suum and Lucina pectinata), *Biochemistry 36*, 13110−13121.
44. Sharma, V. S., and Ranney, H. M. (1978) The dissociation of NO from nitrosylhemoglobin, *J. Biol. Chem. 253*, 6467−6472.
45. Sharma, V. S., Isaacson, R. A., John, M. E., Waterman, M. R., and Chevion, M. (1983) Reaction of nitric oxide with heme proteins: studies on metmyoglobin, opossum methemoglobin, and microperoxidase, *Biochemistry 22*, 3897−3902.

BI7003262